On the instability theory of the melted surface of an ablating body when entering the atmosphere

By SAUL FELDMAN
AVCO Research Laboratory, Everett, Massachusetts

(Received 22 September 1958)

Some ablating bodies entering the atmosphere will melt or soften. Under deceleration, the soft or melted surface will tend to develop instabilities of the Lamb–Taylor type. Two situations involving viscous incompressible fluids are investigated here: one where the liquid layer has constant viscosity and finite thickness, and the other, where the viscosity increases exponentially with distance away from the interface, and the layer is semi-infinite in extent.

It can be demonstrated, that if one neglects gradients in the flow direction, the rate of growth of interface disturbances in a plane normal to the axis of an axially symmetric blunt body is independent of the flow velocity. The fact that the deceleration and liquid thickness vary with time along a trajectory is also included in the analysis. Results of calculations for the amplification factor and the most amplified wavelength are given.

A mechanism due to the deceleration is postulated, which would cause the formation of longitudinal grooves on the surface of an axially symmetric blunt body while entering the atmosphere.

1. Introduction

The possibility of travelling through the Earth's atmosphere at hypersonic speeds has led to the study of heat transfer of ablating objects. Such ablation occurs as a result of the high heat transfer rates encountered in hypersonic flight. Here, the flight time through the atmosphere is short, and in practical applications only part of a properly designed payload envelope will melt or vaporize. An example of some 'good designs' may be seen in plate 1, figure 1 where several stone meteorites that survived the atmospheric journey are shown.

According to their chemical composition meteorites can be classified into irons and stones. Typical elements found in an iron are Fe 91 % and Ni 9 %, by mass, while in stones they find O_2 36 %, Fe 26 %, Si 18 %, Mg 14 %. Since SiO_2, which makes up more than half of the mass of stone meteorites, does not have a definite melting point, stone under re-entry conditions will probably just soften, while irons, on the other hand, will melt.

The attractiveness of using an ablating surface as a heat shield resides in the possibility of vaporizing the soft or melted material. (The problem treated here does not arise in cases where the solid material sublimes.) If the vaporization and melting temperatures differ appreciably, as they do in most substances, the melt must be sufficiently viscous so that it can be heated to the vaporization

temperature before it is swept off the body: thus, the benefit of vaporization will have been realized.

There are two principal mechanisms which may lead to loss of the melted material before deriving the benefit of its evaporation. One is that the liquid, for sufficiently high liquid Reynolds number $W_i\rho_l h/\mu_l$ (where W_i denotes the gas-liquid interface velocity, h the liquid layer thickness, and ρ_l and μ_l denote liquid density and viscosity respectively), could develop instabilities that would lead to liquid entrainment by the gas stream. Due to viscous effects and (or) Helmholtz instability, energy is fed from the main gas stream into the disturbed liquid. The other mechanism is provided by body forces due to deceleration normal to the gas-liquid interface. The softened surface will always have some small-amplitude corrugations at the liquid-gas interface which, under the high deceleration forces normal to the liquid film encountered during re-entry, will amplify and lead to liquid loss. This phenomenon will probably be most important at low liquid Reynolds numbers and in the neighbourhood of the stagnation region of blunt bodies, where the deceleration normal to the body is highest. The component of deceleration parallel to the body only causes a change in the liquid film velocity profile.

A high performance heat shield should avoid or minimize liquid loss due to hydrodynamic instability. The rate of growth of some of these instabilities is investigated here.

Consider the flow about a melting or softening blunt body at zero angle of attack (figure 2). If the radii of curvature are large compared with the liquid layer thickness, a two-dimensional treatment of the problem will be satisfactory. There are two main types of disturbances that have to be investigated: disturbances propagating in the stream direction—in the $(\bar{y}\bar{z})$-plane—and disturbances across the stream in the $(\bar{x}\bar{y})$-plane. Since we are concerned with an efficient heat shield, we will assume that very little material is lost due to hydrodynamic instability during the flight time through the atmosphere, and therefore that the amplification rates must be sufficiently small so that the linear treatment correctly describes the interesting part of the phenomenon. This assumption will have to be checked *a posteriori*.

The treatment of disturbances propagating in the $(\bar{y}\bar{z})$-plane are the subject of the hydrodynamic stability theory of two fluids with body forces normal to the interface. Feldman (1957) treated the problem of the hydrodynamic stability of two fluids with the velocity profile shown in figure 3; the liquid Reynolds numbers were assumed large, and the body forces acted normal to the wall, but in either direction. He found that when the body force was directed towards the wall the flow was destabilized, which seems to disagree with what one would expect intuitively. It was shown that in that problem, gravity—when acting towards the wall—and surface tension produce a Reynolds stress that feeds energy into the disturbance in the case of high liquid Reynolds numbers. In practical applications, however, the liquid Reynolds numbers will be small, and the above-described mechanism will be inoperative; the important destabilizing factor will be the body forces caused by deceleration normal to the gas-liquid interface. Therefore, in this case the velocities in the steady flow (figure 3) can be neglected,

and the problem reduces to one of the type that Lamb (1932) and Taylor (1950) have already investigated.

In other words, in the αR-plane (commonly used for presenting hydrodynamic stability results) at a given wave number, the liquid film is Lamb–Taylor

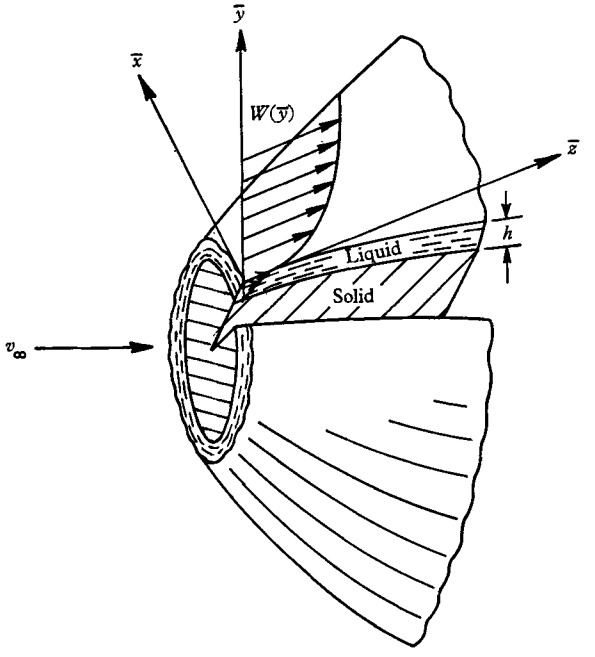

FIGURE 2. Flow about a melting blunt body.

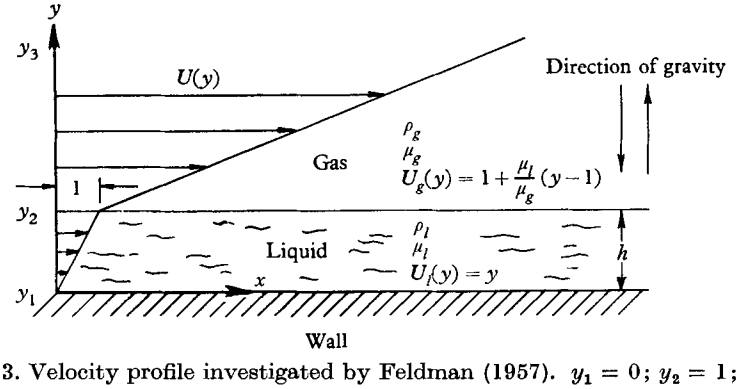

FIGURE 3. Velocity profile investigated by Feldman (1957). $y_1 = 0$; $y_2 = 1$; $y_3 = \infty$.

unstable when the liquid Reynolds number is zero (i.e. no flow). At some small liquid flow rate the film becomes stabilized, and if the flow rate is increased sufficiently, the usual hydrodynamic instability sets in where the body forces away from the solid wall are unimportant compared to shear forces.

We have experimental evidence (to be published elsewhere) that a small amount of gas flow can stabilize Lamb–Taylor instability. The experiment consisted of a horizontal flat plate with a film of silicone in the underface, which

could be inserted into a horizontal air jet. With no gas flow the film would develop the usual Lamb–Taylor columns. At small air flow the spikes would be blown into the gas stream and carried away by it (liquid still unstable). As the gas flow is increased, the columns disappear and instead transverse waves appear of the same wavelength as the columns: these waves seem to be damped since they do not lead to any fluid loss. If the gas flow is increased further, a condition is reached such that the liquid film becomes unstable: liquid blows off the crests of the waves due to the usual high Reynolds number hydrodynamic instability.

The waves that develop as a result of gravity in the liquid film on the underside of an inclined flat plate ('tea-pot' effect) without any gas flow have been shown by Benjamin (1957) to be always unstable. This, however, is not our case when away from the stagnation point of a blunt body, where the shear forces at the gas-liquid interface are far more important than the body forces in determining the liquid velocity profile.

We will therefore assume that in cases of interest, the liquid Reynolds number will be either sufficiently larger than zero, and smaller than the usual critical Reynolds number, so that the disturbances propagating in the $(\bar{y}\bar{z})$-plane are stable, or sufficiently close to zero so that the amplification rate of Lamb–Taylor instability gives an upper limit to the growth rate of disturbances that appear when the liquid flow rate, due to gas-liquid interface shear, is small.

We turn next to investigate the disturbances in the $(\bar{x}\bar{y})$-plane. The hydrodynamic instability of the flow to small two-dimensional disturbances developing in the $(\bar{x}\bar{y})$-plane (figure 2) is investigated theoretically in this paper. As will be pointed out in § 2.1, it is evident that if all z-variations are neglected the instability of this flow is completely independent of the velocity profiles $W(\bar{y})$—in the $(\bar{z})$-direction—of the liquid or gas, and it reduces to the Lamb–Taylor instability problem. Of course, the shape of the perturbed streamlines are a function of $W(\bar{y})$

The initial stages of the Lamb–Taylor instability problem have been treated theoretically in the literature by small perturbation techniques up to the third-order approximation. Experiments have also been carried out in order to check the theories. We will now briefly review the work done on the initial stages of instability.

Lamb (1932, p. 371) pointed out the unstable behaviour of the interface of two semi-infinite inviscid incompressible fluids in a gravitational field normal to their interface, when perturbed by a small oscillation. His results indicate that when the body force acts from the heavier to the lighter fluid the disturbances grow exponentially in time $\bar{t}$, i.e. the ratio of the amplitude η at any time to the original amplitude η_0 is given by

$$\eta/\eta_0 = \exp(\bar{n}\bar{t}), \tag{1}$$

where $\bar{n}$ is the amplification exponent. Lamb also pointed out that the effect of surface tension was to stabilize the motion for wavelengths shorter than a cut-off wavelength $\bar{\lambda}_{co}$, given by

$$\bar{\lambda}_{co} = 2\pi\left[\frac{\sigma}{g(\rho_l - \rho_g)}\right]^{\frac{1}{2}}, \tag{2}$$

where σ is the interfacial surface tension coefficient, g is the acceleration perpendicular to the interface, and the subscripts g and l denote quantities evaluated

for the gas or liquid; the bar denotes dimensional quantities. The wavelength for which the amplification factor $\bar{n}$ is a maximum is called the critical wavelength $\bar{\lambda}_c$, and will be denoted by $\bar{n}_c$.

The result obtained by Lamb for $\bar{n}$, neglecting surface tension, was

$$\bar{n} = \left[\frac{2\pi g}{\bar{\lambda}}\left(\frac{\rho_l - \rho_g}{\rho_l + \rho_g}\right)\right]^{\frac{1}{2}}. \tag{3}$$

Taylor (1950), neglecting surface tension, extended the investigation to include the case where the denser fluid was of finite thickness and the second free surface, although initially flat and stable, was free to distort.

Bellman & Pennington (1954) included viscosity and surface tension in their analysis of two semi-infinite fluids. They found that viscosity had the effect of diminishing the amplification rate $\bar{n}$, but could never by itself make it go to zero for any finite wavelengths. Their calculations have been extended and recast in a more convenient form in § 4.

Chang (1958), by carrying the small disturbance theory to the third order in the amplitude to wavelength ratio, investigated the inviscid problem of one semi-infinite fluid with a free surface in the initial stages of non-linearity. He found a theoretical explanation for an interesting effect due to surface tension, which had been previously observed by Watson (1957), and had been called 'overstability'. Although from Lamb's analysis waves shorter than the cut-off wavelength $\bar{\lambda}_{co}$ are fully stabilized by surface tension (i.e. only oscillatory motion is possible), Watson found experimentally that these waves will oscillate and at the same time grow in amplitude. When including non-linear effects in the theory, Chang found that for $\bar{\lambda} < \bar{\lambda}_{co}$

$$\eta \sim f\eta_0^3 \tau \sin \tau, \tag{4}$$

where

$$\tau = \left[\frac{2\pi g}{\bar{\lambda}}\left(1 - \frac{\bar{\lambda}_{co}}{\bar{\lambda}}\right)\right]^{\frac{1}{2}} \bar{t}, \tag{5}$$

and f is a function $\bar{\lambda}_{co}/\bar{\lambda}$. For $\bar{\lambda} > \bar{\lambda}_{co}$, he checked the result given by (3), and when $\bar{\lambda} = \bar{\lambda}_{co}$ he showed that

$$\eta \sim \eta_0^3 \bar{t}^2.$$

Summarizing, the two essential points in Chang's results are: (1) when the non-linear effects become important, surface tension does not stabilize short wavelengths, although it diminishes their rate of growth; and (2) the critical or maximum rate of growth of disturbances is adequately given by the linear theory that includes surface tension.

Experiments designed to check the linear inviscid theory have been carried out by Lewis (1950), Allred, Blount & Miller (1954), and by Watson (1957). The experimental values of $\bar{n}$ agree within a factor of 1·5, or less, with the theoretical values. Watson found that the agreement of the experimental with the theoretical values of $\bar{n}_c$, at the critical wavelength $\bar{\lambda}_c$, was within 10 %.

Except for Taylor's inviscid finite-thickness layer with two free surfaces, the cases that have been treated in the literature thus far, concerning the Lamb–Taylor instability, involve two fluids of semi-infinite depth and constant viscosity. The cases encountered during re-entry have only one free interface and when the material has a definite melting temperature—like the metals—the liquid has

a finite thickness or, in the case of glasses, the surface softens as the temperature rises.

The rapid increase of viscosity with distance into the solid, or the finite thickness of a molten layer, may reduce its instability to an unimportant problem in the case of certain materials for specific applications. In effect, Chang (1956) has shown that for an inviscid liquid layer of depth h in a vacuum,

$$\bar{n} \sim [\tanh(2\pi h/\bar{\lambda})]^{\frac{1}{2}}, \tag{6}$$

which shows the stabilizing effect of small liquid depths.

2. Instability of a semi-infinite viscous incompressible fluid with an exponential viscosity law

2.1. *Formulation of the problem*

The instability problem of the axisymmetric softened surface of figure 2 will be approximated by the two-dimensional problem represented in figure 4. Let $W(y)$ denote the undisturbed velocity profile. All gradients in the flow direction $\bar{z}$ will

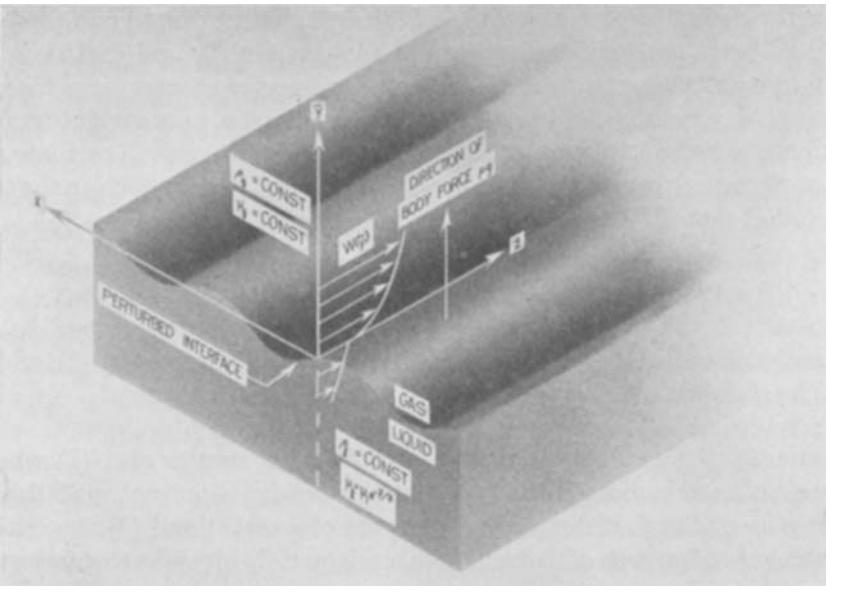

FIGURE 4. Co-ordinate system used in instability calculations.

be neglected. The deceleration causes a body force ρg, normal to the interface and directed from the liquid to the gas. The gas and liquid densities ρ_g and ρ_l, and gas viscosity μ_g, will be assumed constant. The liquid viscosity will be taken as

$$\mu_l = \mu_i e^{-\bar{y}/\delta}, \tag{7}$$

where $\bar{y} \leqslant 0$ for the liquid, and the subscript i indicates a quantity evaluated at the gas-liquid interface. The viscosity law (7) is a good approximation to the behaviour of glassy materials. Specifically, the viscosity of Pyrex during re-entry

heating, was obtained in the interface region (figure 5) from Sutton's (1958) calculations for the temperature distribution through the softening surface. One other justification for using the exponential variation is that it simplifies the analysis considerably.

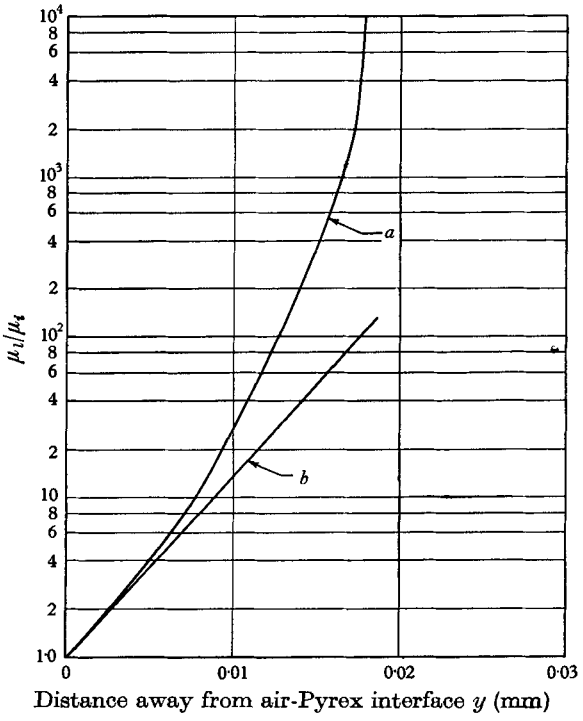

FIGURE 5. Viscosity of Pyrex as a function of distance away from air-Pyrex interface. Interface temperature 4000 °F. Source of data: Sutton (1958). *a*, Obtained by using Sutton's (1958) calculation for the temperature distribution and $\mu = \exp\left(\frac{8720}{T(°\mathrm{R})}\right)^{1\cdot612}$ poises; $T_i = 4460$ °R; $\mu_i = 18\cdot5$ poises. *b*, Exponential approximation.

The relevant dimensionless equations of motion, including body forces in the y-direction, and continuity for an incompressible fluid of variable viscosity, in which the gradients in the z-direction have been neglected, are

$$\frac{\partial u}{\partial t}+u\frac{\partial u}{\partial x}+v\frac{\partial u}{\partial y}=-\frac{\partial p}{\partial x}+\frac{1}{\Re(y)}\left(\frac{\partial^2 u}{\partial x^2}+\frac{\partial^2 u}{\partial y^2}\right)+2\frac{\partial \Re^{-1}}{\partial x}\frac{\partial u}{\partial x}+\frac{\partial \Re^{-1}}{\partial y}\left(\frac{\partial u}{\partial y}+\frac{\partial v}{\partial x}\right), \quad (8)$$

$$\frac{\partial v}{\partial t}+u\frac{\partial v}{\partial x}+v\frac{\partial v}{\partial y}=1-\frac{\partial p}{\partial y}+\frac{1}{\Re(y)}\left(\frac{\partial^2 v}{\partial x^2}+\frac{\partial^2 v}{\partial y^2}\right)+\frac{\partial \Re^{-1}}{\partial x}\left(\frac{\partial v}{\partial x}+\frac{\partial u}{\partial y}\right)+2\frac{\partial \Re^{-1}}{\partial y}\frac{\partial v}{\partial y}, \quad (9)$$

$$\frac{\partial u}{\partial x}+\frac{\partial v}{\partial y}=0, \quad (10)$$

where the subscript l has been deleted and

$$\left.\begin{aligned} u=\bar{u}/U, \quad v=\bar{v}/U, \\ x=\bar{x}/\delta, \quad y=\bar{y}/\delta, \quad z=\bar{z}/\delta, \quad t=\bar{t}U/\delta, \\ U=\sqrt{(g\delta)}, \quad \Re=\rho U\delta/\mu^*, \quad p=\bar{p}/\rho U^2. \end{aligned}\right\} \quad (11)$$

Here u and v are the velocities in the direction of the coordinate axes x and y, p is pressure, g is the acceleration normal to the interface, μ^* is the viscosity and δ is defined by (7). Two further equations could be written down, the equation of motion for the z-direction and an equation for the temperature distribution, but these turn out not to be relevant to the present analysis. The quantities μ_i and δ depend on temperature, of course, but are assumed to be known. Note that equations (8), (9) and (10) do not involve the z-component of velocity, which fact is obviously to be expected as a consequence of our neglect of z-variations.

It will be assumed that the dependent variables can be expanded as

$$\left.\begin{aligned} &u = \epsilon^j u^{(j)}(x,y,t), \quad v = \epsilon^j v^{(j)}(x,y,t), \quad \mu^* = \mu(y) + \epsilon^j \mu^{(j)}(x,y,t), \\ &p = P(y) + \epsilon^j p^{(j)}(x,y,t) \quad (j = 1,2,3,\ldots), \end{aligned}\right\} \tag{12}$$

where ϵ is a small parameter in the problem yet not determined, and the notation of tensor summation has been used.

Inserting (12) and (7) into (8), (9) and (10), and equating coefficients of the first power of ϵ, gives for the first approximation of the disturbed motion

$$\frac{\partial u^{(1)}}{\partial t} = -\frac{\partial p^{(1)}}{\partial x} + \frac{1}{R^{(0)}(y)}\left(\frac{\partial^2 u^{(1)}}{\partial x^2} + \frac{\partial^2 u^{(1)}}{\partial y^2}\right) + \frac{d(R^{(0)})^{-1}}{\partial y}\left(\frac{\partial u^{(1)}}{\partial y} + \frac{\partial v^{(1)}}{\partial x}\right), \tag{13}$$

$$\frac{\partial v^{(1)}}{\partial t} = -\frac{\partial p^{(1)}}{\partial y} + \frac{1}{R^{(0)}(y)}\left(\frac{\partial^2 v^{(1)}}{\partial x^2} + \frac{\partial^2 v^{(1)}}{\partial y^2}\right) + 2\frac{d(R^{(0)})^{-1}}{\partial y}\frac{\partial v^{(1)}}{\partial y}, \tag{14}$$

$$\frac{\partial u^{(1)}}{\partial x} + \frac{\partial v^{(1)}}{\partial y} = 0, \tag{15}$$

where

$$R^{(0)} = \rho U \delta / \mu(y). \tag{16}$$

Equations (13), (14) and (15) form a system for the three unknowns, $u^{(1)}$, $v^{(1)}$ and $p^{(1)}$. Since the system does not contain $W(y)$, the motion in the (xy)-plane and the solution of the stability problem are independent of the cross velocity $W(y)$, regardless of the viscosity law that is used.

2.2. *Boundary conditions. Derivation of the disturbance equation*

In order to simplify the calculation, we will replace the gas (figure 4) by a vacuum, i.e. $\rho_g = 0$. Equation (3) shows that this is a very good approximation. Therefore, all quantities in the analysis from here on will refer to the behaviour of the liquid.

The boundary conditions applicable to (13), (14) and (15) will be written in dimensionless form. At the interface ($y = y_i$), the tangential stress vanishes, i.e.

$$\frac{\partial u^{(1)}}{\partial y} + \frac{\partial v^{(1)}}{\partial x} = 0, \tag{17}$$

and the normal stress is in equilibrium with the surface tension; thus,

$$-p^{(1)} + \frac{2}{R}\frac{\partial v^{(1)}}{\partial y} - \frac{1}{W}\frac{\partial^2 y_i^{(1)}}{\partial x^2} = 0, \tag{18}$$

where the subscript i denotes interface, and R and W are the interface Reynolds and Weber numbers given by

$$R = \rho g^{\frac{1}{2}} \delta^{\frac{3}{2}} / \mu_i \quad \text{and} \quad W = g\delta^2 \rho / \sigma, \tag{19}$$

where σ is the surface tension coefficient.

As $y \to -\infty$, the disturbance must vanish, i.e.

$$v^{(1)} = 0, \quad u^{(1)} = 0. \tag{20}$$

Let ζ denote the vorticity of the perturbed flow, i.e.

$$\zeta = \frac{\partial v^{(1)}}{\partial x} - \frac{\partial u^{(1)}}{\partial y}. \tag{21}$$

From (15) and (21),

$$\nabla^2 u^{(1)} = -\frac{\partial \zeta}{\partial y}, \quad \text{where} \quad \nabla^2 \equiv \frac{\partial^2}{\partial x^2} + \frac{\partial^2}{\partial y^2}. \tag{22}$$

Differentiating (14) and (13) with respect to x and y, respectively, subtracting the second result from the first, and using (22), it follows that

$$R^{(0)} \frac{\partial \zeta}{\partial t} = \nabla^2 \zeta - 2 \frac{d \log R^{(0)}}{\partial y} \frac{\partial \zeta}{\partial y} + \left[2 \left(\frac{d \log R^{(0)}}{\partial y} \right)^2 - \frac{1}{R^{(0)}} \frac{d^2 R^{(0)}}{\partial y^2} \right] \left(\zeta - 2 \frac{\partial v^{(1)}}{\partial x} \right). \tag{23}$$

The equation of continuity assures the existence of a stream function ψ such that

$$u^{(1)} = \psi_y \quad \text{and} \quad v^{(1)} = -\psi_x, \tag{24}$$

the subscripts denoting partial derivatives. We now choose as the representation of the disturbance stream function

$$\psi = \Phi(y)\, e^{i\alpha x + nt}, \tag{25}$$

where the wave-number α and the amplification exponent n are given by

$$\alpha = 2\pi/\lambda = 2\pi\delta/\bar{\lambda}, \quad n = \bar{n} \sqrt{(\delta/g)}. \tag{26}$$

From (24) and (25), the disturbance velocities and the vorticity can be written as

$$u^{(1)} = \Phi'(y)\, e^{i\alpha x + nt}, \quad v^{(1)} = i\alpha \Phi\, e^{i\alpha x + nt}, \tag{27}$$

$$\zeta = -(\Phi'' - \alpha^2 \Phi)\, e^{i\alpha x + nt}. \tag{28}$$

If we write $d/dy \equiv D$, $\nabla^2 \zeta$ becomes

$$\nabla^2 \zeta = -(D^2 - \alpha^2)^2\, \Phi\, e^{i\alpha x + nt},$$

which, together with (7) and (16), can be inserted into (23) to yield

$$\{[(D-1)^2 - \alpha^2](D^2 - \alpha^2) + 2\alpha^2\}\, \Phi = nR\, e^y (D^2 - \alpha^2)\, \Phi, \tag{29}$$

where R is given by (19). Note that the right-hand member of (29) is proportional to $\partial\zeta/\partial t$.

The boundary conditions on Φ in (29) will now be obtained from (17), (18) and (20). We will first express $\partial^2 y_i^{(1)}/\partial x^2$ and $p^{(1)}$ that appear in (18).

At the interface, for small slopes,

$$\frac{\partial y_i^{(1)}}{\partial t} = v_i^{(1)} = -i\alpha \Phi\, e^{i\alpha x + nt}. \tag{30}$$

The shape of the interface may be expressed as

$$y_i^{(1)} = \hat{y}_i e^{i\alpha x+nt}, \tag{31}$$

where y_i is the complex amplitude. Insertion of (31) into (30) gives

$$y_i = -i\frac{\alpha}{n}\Phi(0)\, e^{i\alpha x+nt}, \tag{32}$$

and

$$\frac{\partial^2 y_i^{(1)}}{\partial x^2} = i\frac{\alpha^3}{n}\Phi(0)\, e^{i\alpha x+nt}. \tag{33}$$

In order to determine $p^{(1)}$, let

$$p^{(1)} = \hat{p}(y)\, e^{i\alpha x+nt}, \tag{34}$$

which, together with (27), can be inserted into (13) to yield, when evaluated at the disturbed interface y_i,

$$\hat{p} = -\frac{i}{\alpha R}[\Phi'''(0) - \Phi''(0) - (nR+\alpha^2)\,\Phi'(0) - \alpha^2\Phi(0)]. \tag{35}$$

We have thus managed to integrate the (x)-momentum equation of $O(\epsilon)$ in order to obtain $p^{(1)}$. There still may be lacking a constant of integration. In effect, integration with respect to y of the complete equation given by (9), would yield, at the disturbed interface y_i a term of $O(\epsilon)$ which comes from the term of $O(1)$. This additional term is precisely y_i, which from (32) is

$$y_i = -i\frac{\alpha}{n}\Phi(0)\, e^{i\alpha x+nt}. \tag{36}$$

From (34), (35) and (36), $p^{(1)}$ at the interface is

$$p^{(1)} = -\frac{i}{\alpha R}\left[\Phi'''(0) - \Phi''(0) - (nR+\alpha^2)\,\Phi'(0) + \alpha^2\left(\frac{R}{n}-1\right)\Phi(0)\right] e^{i\alpha x+nt}. \tag{37}$$

When inserting (27), (33) and (37) into (17), (18) and (20), these become at $y = 0$

$$\Phi'' + \alpha^2\Phi = 0, \tag{38}$$

$$\Phi''' - \Phi'' - (nR+3\alpha^2)\,\Phi' + \alpha^2\left[\frac{R}{n}\left(1-\frac{\alpha^2}{W}\right)-1\right]\Phi = 0.$$

Inserting (38) into the last expression gives

$$\Phi''' - (nR+3\alpha^2)\,\Phi' + \alpha^2\frac{R}{n}\left(1-\frac{\alpha^2}{W}\right)\Phi = 0. \tag{39}$$

At $y = -\infty$, we have $\Phi = 0$ and $\Phi' = 0$. (40)

2.3. *Solution of the disturbance equation for* $nR \gg 1$

For $nR \gg 1$, (29) reduces to the inviscid case. Since the fourth-order equation reduces to one of second order, two of the boundary conditions cannot be retained; i.e. (38) and the second of (40). The eigenvalue for n then reduces to (80) below.

2.4. *Solution of the disturbance equation for* $nR \ll 1$

The disturbance equation (29) whose boundary conditions are given by (38), (39) and (40), will now be solved. We will assume that $nR \ll 1$ and expand Φ in a power series in nR, i.e.

$$\Phi = \sum_{k=0}^{\infty} (nR)^k \Phi^{(k)}. \tag{41}$$

Physically, $nR \ll 1$ means that the amplification exponent $\bar{n}$ satisfies

$$\bar{n} \ll \frac{\mu_i}{\rho \delta^2}. \tag{42}$$

The correctness of the assumption that the product nR is small will have to be checked *a posteriori*, when calculations are made for specific instability situations.

Substituting (41) into (29), (38), (39) and (40) gives the differential equation for the first approximation to Φ

$$\{[(D-1)^2-\alpha^2](D^2-\alpha^2)+2\alpha^2\}\Phi^{(0)} = 0, \tag{43}$$

with the boundary conditions at $y = 0$

$$\Phi^{(0)''} + \alpha^2 \Phi^{(0)} = 0, \tag{44}$$

$$\Phi^{(0)'''} - 3\alpha^2 \Phi^{(0)'} + \alpha^2 \frac{R}{n}\left(1 - \frac{\alpha^2}{W}\right)\Phi^{(0)} = 0, \tag{45}$$

and at $y = -\infty$

$$\Phi^{(0)} = 0 \quad \text{and} \quad \Phi^{(0)'} = 0. \tag{46}$$

Since the right-hand member of (43) vanishes, this is tantamount to neglecting in (23) the time rate of change of vorticity. (43) is an ordinary linear fourth-order differential equation with constant coefficients; its solutions are of the form

$$\Phi_j^{(0)} = \exp(q_j + \tfrac{1}{2}), \tag{47}$$

where the q_j's are given by

$$q_1 = (\alpha^2 + \tfrac{1}{4} + i\alpha)^{\frac{1}{2}}, \quad q_2 = q_1^*, \quad q_3 = -q_1, \quad q_4 = -q_1^*, \tag{48}$$

and where the stars denote complex conjugates. If we let

$$A = [(1+4\alpha^2)^2 + 16\alpha^2]^{\frac{1}{4}}, \quad \chi = \tan^{-1}\left(\frac{4\alpha}{1+4\alpha^2}\right), \tag{49}$$

$$\left.\begin{aligned} \xi &= A\cos\tfrac{1}{2}\chi = \sqrt{\left[\frac{A^2+(1+4\alpha^2)}{2}\right]}, \\ \text{and} \qquad \eta &= A\sin\tfrac{1}{2}\chi = \sqrt{\left[\frac{A^2-(1+4\alpha^2)}{2}\right]}, \end{aligned}\right\} \tag{50}$$

it can be shown that the solution of (43) can be written as

$$\Phi^{(0)} = \sum_{j=1}^{4} k_j \Phi_j^{(0)}, \tag{51}$$

where

$$\Phi_1^{(0)} = \exp[\tfrac{1}{2}(1+\xi+i\eta)y], \quad \Phi_2^{(0)} = \Phi_1^{(0)*}, \tag{52}$$

$$\Phi_3^{(0)} = \exp[\tfrac{1}{2}(1-\xi-i\eta)y], \quad \Phi_4^{(0)} = \Phi_3^{(0)*} \qquad (y \leqslant 0). \tag{53}$$

In order to satisfy the boundary conditions (46), $k_3 = k_4 = 0$. Therefore we have

$$\Phi^{(0)} = k_1 \Phi_1^{(0)} + k_2 \Phi_2^{(0)}, \tag{54}$$

which when substituted into (44) and (45) gives

$$\left.\begin{aligned} k_1(s^2+\alpha^2) + k_2(s^{*2}+\alpha^2) &= 0, \\ k_1\left[s^3 - 3\alpha^2 s + \alpha^2 \frac{R}{n}\left(1-\frac{\alpha^2}{W}\right)\right] + k_2\left[s^{*3} - 3\alpha^2 s^* + \alpha^2 \frac{R}{n}\left(1-\frac{\alpha^2}{W}\right)\right] &= 0, \end{aligned}\right\} \tag{55}$$

where $$s = \tfrac{1}{2}(1+\xi+i\eta) \quad \text{and} \quad s^* = \tfrac{1}{2}(1+\xi-i\eta). \tag{56}$$

Since k_1 and k_2 are non-vanishing, (55) requires that

$$\begin{vmatrix} s^2+\alpha^2 & s^{*2}+\alpha^2 \\ s^3 - 3\alpha^2 s + \alpha^2 \frac{R}{n}\left(1-\frac{\alpha^2}{W}\right) & s^{*3} - 3\alpha^2 s^* + \alpha^2 \frac{R}{n}\left(1-\frac{\alpha^2}{W}\right) \end{vmatrix} = 0, \tag{57}$$

which is the eigenvalue determinant that describes the instability of the flow. Solving (57) for n/R yields

$$\frac{n}{R} = \frac{2 s_r \alpha^2 (1-\alpha^2/W)}{(s_r^2+s_i^2)^2 + \alpha^2(6s_r^2+2s_i^2-3\alpha^2)}, \tag{58}$$

where $$s_r = \tfrac{1}{2}(1+\xi), \quad s_i = \tfrac{1}{2}\eta. \tag{59}$$

Further, ζ and η are given by (50). From (58) it can be seen that as $\alpha \to 0$, $n/R \to 0$; and also $n/R = 0$ at the cut-off wave number,

$$\alpha_{co} = \sqrt{W}, \tag{60}$$

which agrees with (2). The curve of n/R *vs* α then has a maximum at a wave-number smaller than the cut-off wave number. For sufficiently small wave numbers, n/R is independent of W.

2.5. *Limiting form of* (58) *for* $\alpha \ll 1$

For small values of the wave-number α, it follows, from (49), (50) and (59), that

$$A^2 = 1 + 12\alpha^2 + O(\alpha^4), \quad s_r^2 = 1 + 4\alpha^2 + O(\alpha^4) \quad \text{and} \quad s_i^2 = \alpha^2 + O(\alpha^4). \tag{61}$$

Inserting (65) into (62) gives

$$n/R = 2\alpha^2(1-\alpha^2/W)[1 - 14\alpha^2 + O(\alpha^4)]. \tag{62}$$

Differentiating (62) with respect to α and setting the result equal to zero, yields the critical wave-number α_c that will maximize the value n/R, i.e.

$$\alpha_c = \frac{1+O(\alpha_c^4)}{\sqrt{\{2(14+1/W)\}}}. \tag{63}$$

Substituting (63) into (62) gives, up to terms of $O(\alpha^4)$,

$$n_c/R = \frac{1}{G}\left(1 - \frac{1}{2WG}\right)\left(1 - \frac{7}{G}\right), \tag{64}$$

where $G = 14 + 1/W$.

For small W, (62), (63) and (64) give respectively

$$n/R = 2\alpha^2, \quad \alpha_c = \sqrt{(\tfrac{1}{2}W)}, \quad n_c/R = \tfrac{1}{2}W. \tag{65}$$

Thus, when W is small, (60) and (65) determine the important features of the amplification exponent; these are summarized in figure 6.

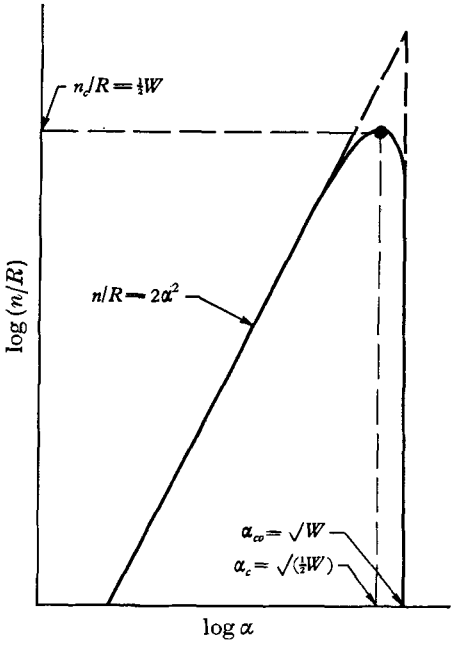

FIGURE 6. Important features of the amplification exponent for small values of α and W and exponential viscosity variation in a liquid of infinite depth.

For large W, α_c is of $O(1)$, and no significant simplification of (58) can be made.

Since for some materials, the case of small α and W may be of considerable practical importance, (60) and (65) will be restated, for convenience, in dimensional form; thus

$$\bar{\lambda}_{co} = 2\pi\sqrt{(\sigma/\rho g)}, \quad \bar{\lambda}_c = \sqrt{2}\,\bar{\lambda}_{co}, \tag{66}$$

$$\bar{n}_c = \frac{(\rho g)^2\delta^3}{2\sigma\mu_i}. \tag{67}$$

Since for high-performance heat shields, the amplification factor $\bar{n}$ has to remain small, (67) shows clearly the importance of having large viscosity and surface tension, as well as a rapid change of viscosity with distance (i.e. small δ).

2.6. *Limiting form of* (58) *for* $\alpha \gg 1$

In this case it can be shown that if $\alpha^2/W \ll 1$ and $\alpha \gg 1$, (62) reduces to

$$n/R = 1/(2\alpha). \tag{68}$$

Finally, (58) is plotted in figure 7, where the Weber number W is a parameter. Note that for $\alpha \gg 1$, (68) agrees with the plot. The critical values, as read from

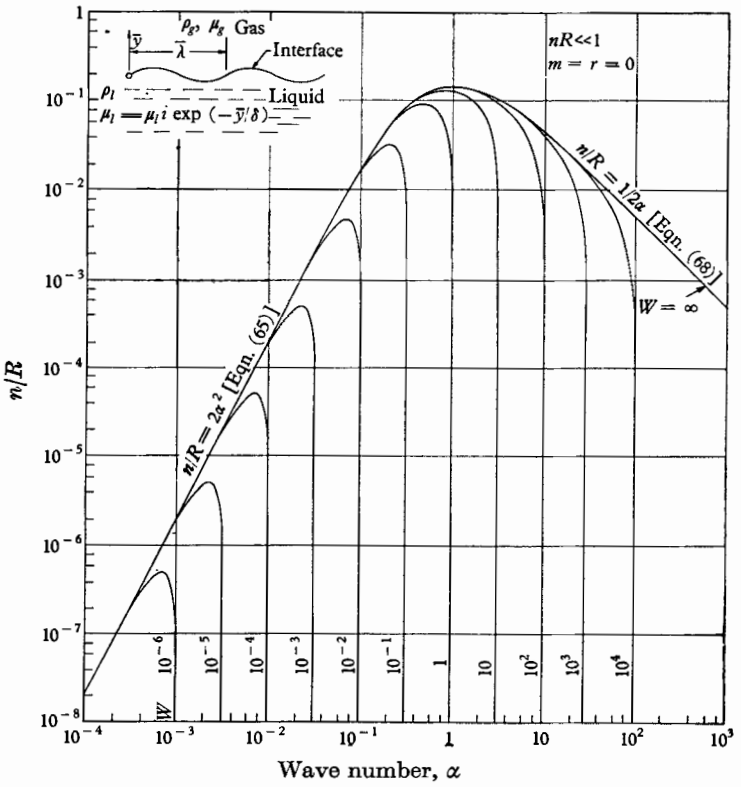

FIGURE 7. Amplification exponent for a liquid of infinite depth and exponential viscosity variation ($nR \ll 1$). $\alpha = 2\pi\delta/\bar{\lambda}$; $m = \mu_g/\mu_l$; $r = \rho_g/\rho_l$; $R = \sqrt{g\rho_l\delta^3}/\mu_l$; $W = g\rho_l\delta^2/\sigma$; n = amplification exponent.

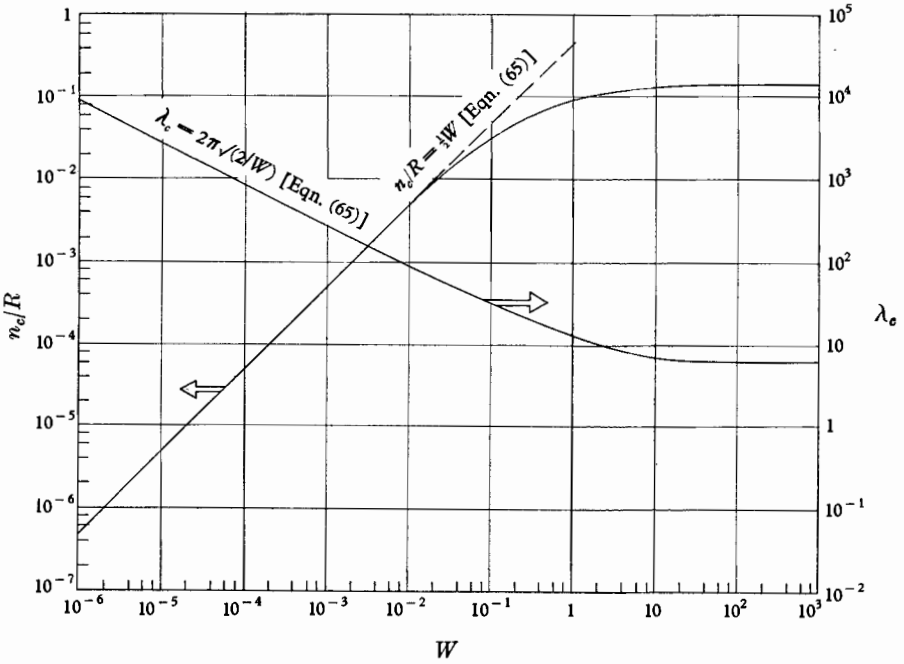

FIGURE 8. Critical wavelength $\bar{\lambda}_c$ and amplification exponent n_c as determined from figure 7.

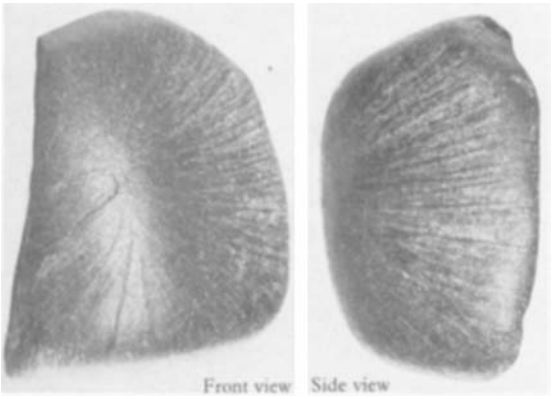

Purdue, Lafayette, Indiana

Whitman, Nebraska (stone)
found 1937
Courtesy of the Mininger Collection of Meteorites, Winslow, Arizona

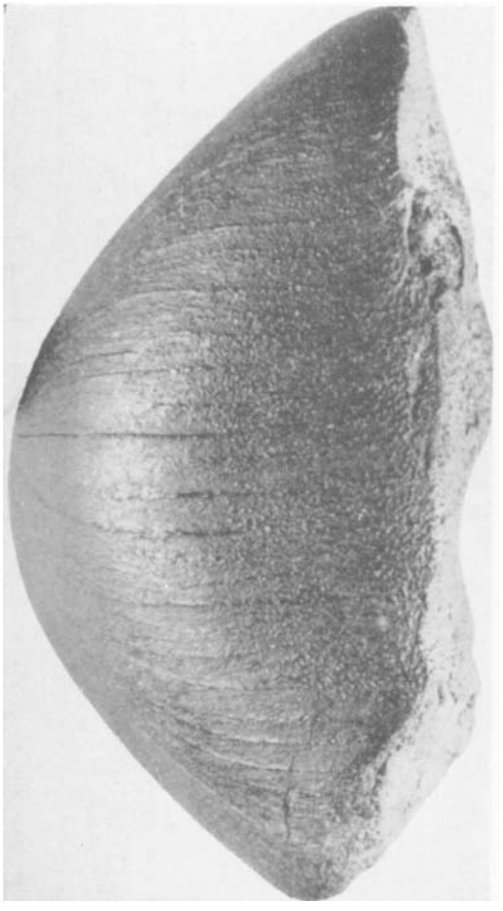

Lafayette, Ind. (stone) known before 1931
Courtesy of Purdue University

Princetown, Highland Co., Ohio (stone)
fell in 1893
Courtesy of the American Museum of Natural History

FIGURE 1. Photograph of some stone meteorites that 'successfully' entered the atmosphere.

FELDMAN

(*Facing p.* 144)

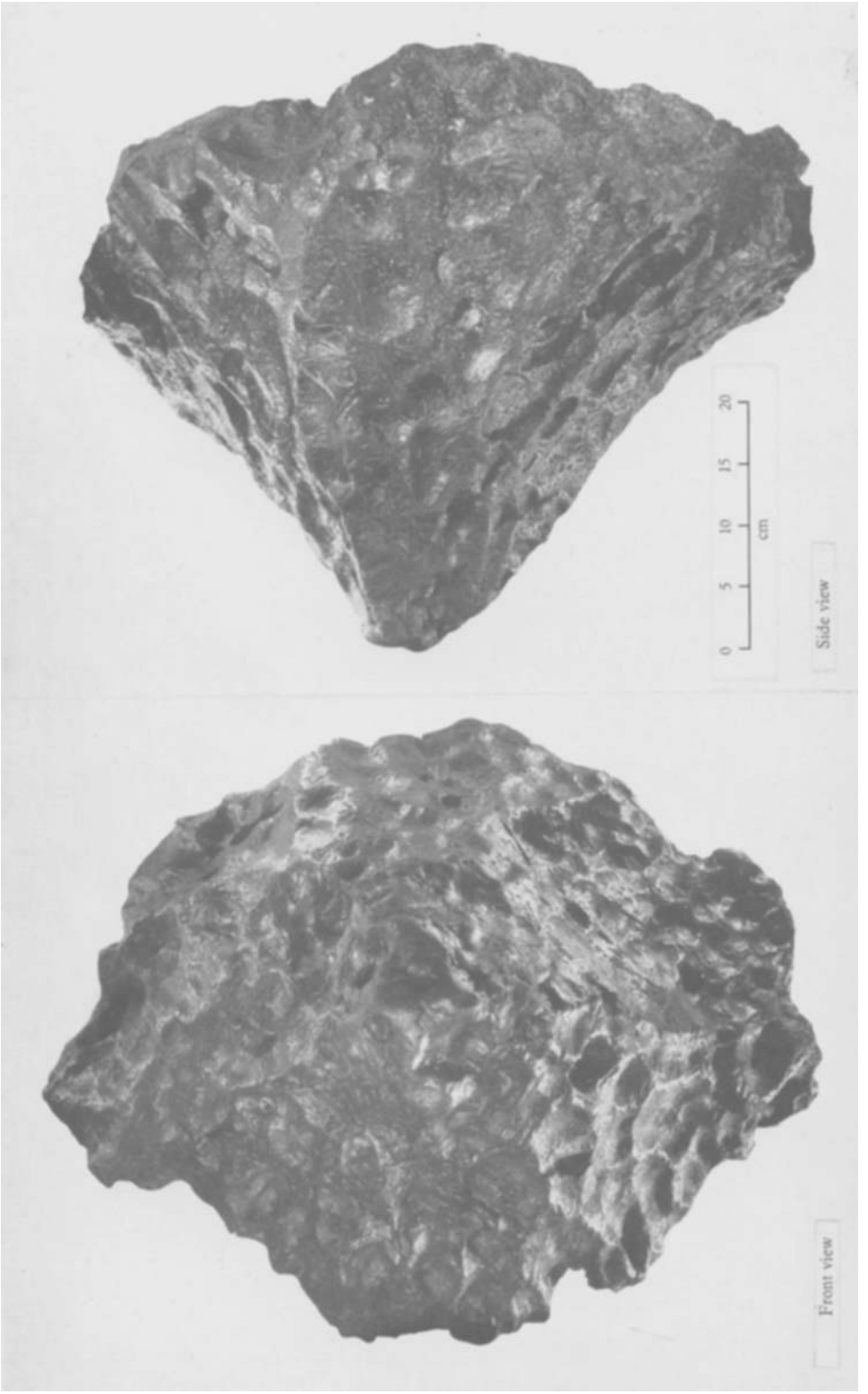

FIGURE 14. Photograph of the Grant, New Mexico, iron meteorite, found about 1929, showing flow markings.

figure 7 have been plotted in figure 8, where a comparison is made with (65) for small values of W. Figure 8 could be obtained analytically by maximizing n/R with respect to α in (58).

3. Instability of a viscous incompressible fluid of finite thickness and constant viscosity

We will now modify the previous analysis so that it may be applied to a class of materials that have a definite melting temperature and whose viscosity has a weak temperature dependence. In this case the viscosity will be assumed to remain constant across the liquid layer.

3.1. *Derivation of the eigenvalue determinant*

The present problem differs from the case discussed in § 2 by the fact that the liquid layer has a constant viscosity μ, and a finite thickness h.

The differential equation (23) simplifies to

$$R\frac{\partial\zeta}{\partial t} = \nabla^2\zeta, \tag{69}$$

with

$$R = \rho g^{\frac{1}{3}} h^{\frac{2}{3}}/\mu, \tag{70}$$

$$y = \bar{y}/h \quad \text{and} \quad x = \bar{x}/h. \tag{71}$$

Instead of (29) we now obtain

$$[(D^2-\alpha^2)^2 - nR(D^2-\alpha^2)]\,\Phi = 0 \tag{72}$$

with the boundary conditions given as before by (38) and (39), while here (40) holds at $y = -1$ instead of negative infinity; i.e. at $\bar{y} = -h$

$$\Phi = 0, \quad \Phi' = 0. \tag{73}$$

Although the differential equation is simpler than before, the eigenvalue determinant here will be more cumbersome due to the boundary condition (73).

The solution of (72) is given by

$$\Phi = k_1 e^{-\alpha y} + k_2 e^{-\beta y} + k_3 e^{\alpha y} + k_4 e^{\beta y}, \tag{74}$$

where

$$\beta = \sqrt{(\alpha^2 + nR)}. \tag{75}$$

Since k_1, k_2, k_3 and k_4 are non-vanishing, substituting (74) into the boundary conditions (38), (39) and (73) yields

$$\begin{vmatrix} e^{\alpha} & e^{\beta} & e^{-\alpha} & e^{-\beta} \\ -\alpha e^{\alpha} & -\beta e^{\beta} & \alpha e^{-\alpha} & \beta e^{-\beta} \\ \left[\alpha(nR+2\alpha^2) + \alpha^2\frac{R}{n}\left(1-\frac{\alpha^2}{W}\right)\right] & \left[-\beta^3+\beta(nR+3\alpha^2) + \alpha^2\frac{R}{n}\left(1-\frac{\alpha^2}{W}\right)\right] & \left[-\alpha(nR+2\alpha^2) + \alpha^2\frac{R}{n}\left(1-\frac{\alpha^2}{W}\right)\right] & \left[\beta^3-\beta(nR+3\alpha^2) + \alpha^2\frac{R}{n}\left(1-\frac{\alpha^2}{W}\right)\right] \\ 2\alpha^2 & \alpha^2+\beta^2 & 2\alpha^2 & \alpha^2+\beta^2 \end{vmatrix} = 0. \tag{76}$$

This equation can be shown to reduce to

$$\frac{1}{4\gamma}\left[-4\beta+\alpha\gamma^2-\left(\frac{R}{\alpha}\right)^2\left(1-\frac{\alpha^2}{W}\right)\right]\left[\left(\frac{1}{\alpha}+\frac{1}{\beta}\right)\sinh(\alpha+\beta)-\left(\frac{1}{\alpha}+\frac{1}{\beta}\right)\sinh(\beta-\alpha)\right]$$

$$+e^{-(\alpha+\beta)}\left[\frac{\gamma}{4}\left(1-\frac{\alpha}{\beta}\right)+\frac{1}{\gamma}\left(1-\frac{\beta}{\alpha}\right)\right]+\frac{e^{-(\beta-\alpha)}}{\gamma}\left(1+\frac{\beta}{\alpha}\right)+e^{(\beta-\alpha)}\frac{\gamma}{4}\left(1+\frac{\alpha}{\beta}\right)-2=0, \quad (77)$$

where

$$\gamma = 2+Rn/\alpha^2. \quad (78)$$

Prior to presenting (77) in graphical form, we will discuss its behaviour for some limiting cases.

3.2. *Some limiting forms of the eigenvalue determinant* (77) *and comparison with the liquid layer of semi-infinite depth*

As $R \to \infty$, (77) reduces to

$$n = [\alpha(1-\alpha^2/W)\tanh\alpha]^{\frac{1}{2}}. \quad (79)$$

The tanh α dependence in (79) agrees with (6), which was obtained by Chang (1956). Note that for large α, i.e. small $\bar{\lambda}/h$, (79) reduces to the case of a liquid layer of infinite depth:

$$n = [\alpha(1-\alpha^2/W)]^{\frac{1}{2}}. \quad (80)$$

For small α, we have from (79)

$$n = \alpha, \quad \text{or} \quad \bar{n} = \frac{2\pi}{\bar{\lambda}}\sqrt{(gh)}, \quad (81)$$

while for the deep liquid layer

$$n = \sqrt{\alpha}, \quad \text{or} \quad \bar{n} = \sqrt{(2\pi g/\bar{\lambda})}. \quad (82)$$

From (79) the critical values cannot, in general, be written explicitly since transcendental expressions are involved. These can be reduced, for the case of small α, to

$$n_c = \sqrt{(\tfrac{1}{2}W)}, \quad \text{and} \quad \alpha_c = \sqrt{(\tfrac{1}{2}W)}, \quad (83)$$

or

$$\bar{n}_c = \tfrac{1}{2}(\rho h/\sigma)^{\frac{1}{2}}g \quad \text{and} \quad \bar{\alpha}_c = \frac{1}{\sqrt{2}}(\rho g/\sigma)^{\frac{1}{2}}, \quad (84)$$

while for the semi-infinite fluid (Bellman & Pennington 1954) the critical values are given by

$$n_c = [\tfrac{2}{3}\sqrt{(\tfrac{1}{3}W)}]^{\frac{1}{2}} \quad \text{and} \quad \alpha_c = \sqrt{(\tfrac{1}{3}W)}, \quad (85)$$

or

$$\bar{n}_c = (2/3)^{\frac{1}{2}}(\rho/3\sigma)^{\frac{1}{4}}g^{\frac{3}{4}} \quad \text{and} \quad \bar{\alpha}_c = 3^{-\frac{1}{2}}(\rho g/\sigma)^{\frac{1}{2}}. \quad (86)$$

3.3. *The behaviour of the amplification exponent for a fluid of finite thickness*

Figure 9 is a plot of (77). The curve for $R = \infty$ coincides with (79) and for small α with (81).

For small values of α, in the inviscid case ($R = \infty$), the closer the wall is to the interface, the smaller the amplification exponent; the presence of the wall decreases the amplification of the disturbances. When viscosity is included, the wall has yet a more important damping effect, because it forces to zero the

u-component of the disturbance velocity. The larger the viscosity, the stronger this effect. It can also be shown, from (77), that for sufficiently small values of α

$$n \sim \alpha^2. \tag{87}$$

For large values of α, the wall should have no effect, the results should coincide with the semi-infinite fluid (figures 10, 11), and since large α means also high spatial frequency, viscosity becomes effective in diminishing the amplification rate.

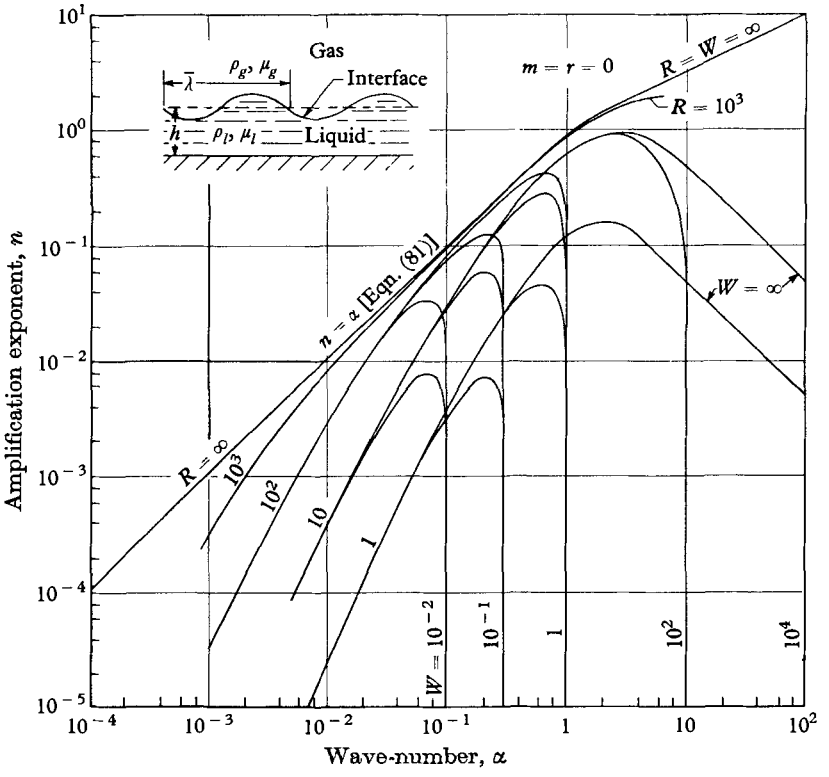

FIGURE 9. Amplification exponent for a liquid of finite depth and constant viscosity. $\alpha = 2\pi h/\lambda$; $m = \mu_g/\mu_l$; $r = \rho_g/\rho_l$; $R = \sqrt{g}\,\rho_l h^{\frac{3}{2}}/\mu_l$; $W = g\rho_l h^2/\sigma$.

For small nR, from figure 9, it seems that

$$n/R = 0{\cdot}2\alpha^2 \tag{88}$$

is probably a good approximation. Comparing (88) with the similar expression (65) for the semi-infinite fluid with an exponential variation of viscosity, we conclude that if

$$h/\delta = 10^{\frac{1}{3}}, \tag{89}$$

a disturbance of the same wavelength in each problem, will grow at the same rate per unit time. The restrictions on (89) are that nR and $\alpha \ll 1$.

4. Instability of a viscous incompressible fluid of semi-infinite depth and constant viscosity

For the sake of completeness, the calculations of Bellman & Pennington (1954) for a fluid of semi-infinite depth have been extended, and the results are presented in a more convenient form than given by these authors. Here we use dimensionless parameters, the characteristic length h, being completely arbitrary.

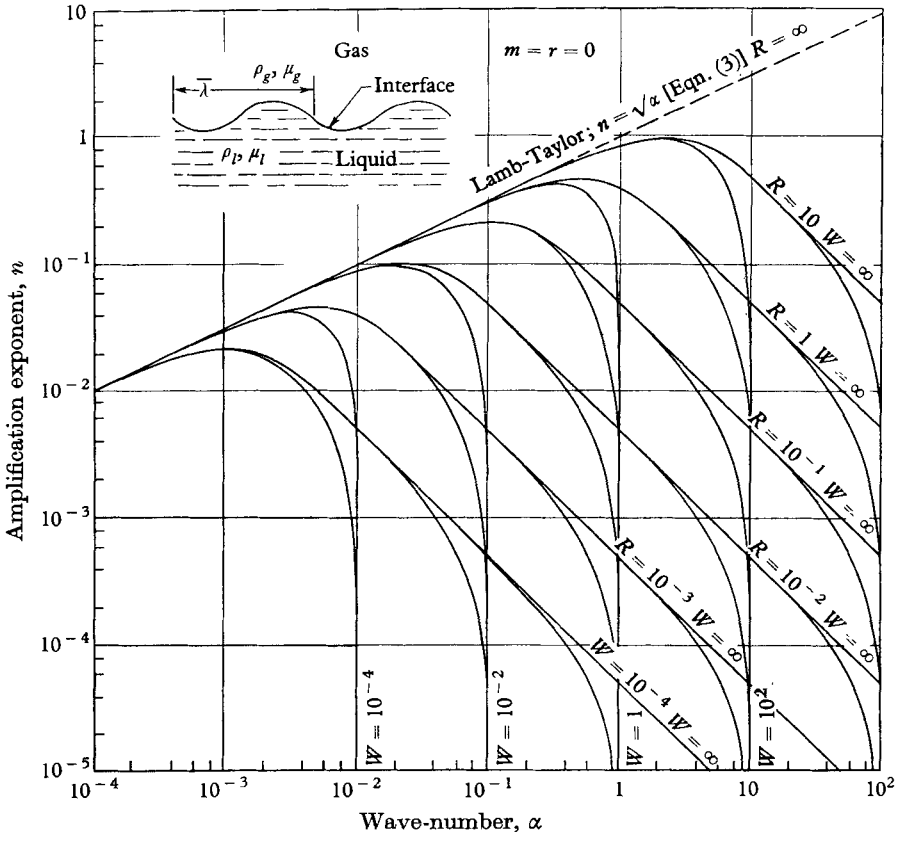

FIGURE 10. Amplification exponent for a liquid of infinite depth and constant viscosity. $\alpha = 2\pi h/\bar{\lambda}$; $m = \mu_g/\mu_l$; $r = \rho_g/\rho_l$; $R = \sqrt{g\rho_l h^3}/\mu_l$; $W = g\rho_l h^2/\sigma$; h = arbitrary reference length.

The implicit expression for n in terms of α is

$$\left[n^2 - \alpha\left(1 - \frac{\alpha^2}{W}\right)\right]\left(1 + \frac{1}{1 + nR/\alpha^2}\right) + 4\alpha^2 n/R = 0, \tag{90}$$

and n is given as a function of α in figure 10 where R and W are parameters. Given the values of g, ρ_l, μ_l and σ, the freedom in the choice of the reference length h allows an adjustment of the values of R and W so that figure 10 can always be used for any physical situation.

Note that when $\alpha^2/nR \ll 1$, (90) reduces to the inviscid curve of Lamb–Taylor given by (3). This, of course, follows since $\alpha^2/nR \ll 1$ is equivalent to low values of viscosity, i.e. inviscid motion.

In order to give an indication of the stabilizing effect of the presence of a wall close to the liquid free surface, we can compare figures 9 and 10 for given α, R and W, by using the same value of h in figure 10 as is used in figure 9. Then, the ratio of the n's for both cases becomes identical to the ratio of the dimensional $\bar{n}$'s. The decrease in the value of the amplification exponent $\bar{n}$, due to the finite thickness h, can easily be noted, especially for small values of α.

If surface tension is negligible, i.e. $W = \infty$, and if $nR/\alpha^2 \gg 1$, the critical values can be obtained from (90) as

$$n_c = R^{\frac{1}{3}}/4^{\frac{2}{3}} \quad \text{and} \quad \alpha_c = R^{\frac{2}{3}}/(32)^{\frac{1}{3}}, \tag{91}$$

or

$$\bar{n}_c = 4^{-\frac{2}{3}}(\rho/\mu)^{\frac{1}{3}} g^{\frac{2}{3}} \quad \text{and} \quad \bar{\alpha}_c = (\rho/\mu)^{\frac{2}{3}} g^{\frac{1}{3}}/(32)^{\frac{1}{3}}. \tag{92}$$

Although $n_c R/\alpha_c^2 = 4$ and not $\gg 1$, the agreement of (91) with the results of figure 10 is satisfactory.

From figures 9 and 10 it can be seen that for a given value of R, both curves have the same asymptotic behaviour for large values of α, as remarked in § 3.3.

5. Summary of the critical quantities for some of the cases considered

As we have seen, the maximum amplification exponent for a given physical situation cannot always be expressed in simple analytical form. However, the cases for which this can be done are summarized in table 1, where we present the maximum amplification exponent $\bar{n}_{cr}$, and the wavelength $\bar{\lambda}_{cr}$ at which it occurs, as a function of the dimensional quantities that arise in the problem.

Case no.	Case restrictions	Equation no. in text	$\bar{n}_c$	$\bar{\lambda}_c$
1	$\mu = 0, h = \infty$	(86)	$\sqrt{(2/3)}\,(\rho/3\sigma)^{\frac{1}{2}} g^{\frac{3}{4}}$	$\sqrt{(3\lambda_0)}$
2	$\sigma = 0, \mu = \text{const}, h = \infty$	(92)	$4^{-\frac{2}{3}}(\rho/\mu)^{\frac{1}{3}} g^{\frac{2}{3}}$	$2\pi(32)^{\frac{1}{3}}(\mu/\rho)^{\frac{2}{3}} g^{-\frac{1}{3}}$
3	$\mu = 0, h/\bar{\lambda} \ll 1$	(84)	$\frac{1}{2}(\rho h/\sigma)^{\frac{1}{2}} g$	$\sqrt{2}\,\bar{\lambda}_{co}$
4	$\mu = \mu_i\, e^{-\nu/\delta}$, $\delta/\bar{\lambda} \ll 1$, $\bar{n}\rho\delta^2\mu_i \ll 1$	(66), (67)	$\frac{1}{2}(\rho g)^2\, \delta^3/\sigma\mu_i$	$\sqrt{2}\,\bar{\lambda}_{co}$

TABLE 1. Résumé of the critical quantities for some of the instability cases considered; $\bar{\lambda}_{co} = 2\pi(\sigma/\rho g)^{\frac{1}{2}}$.

Note that when surface tension is non-vanishing, it will usually control the size of the critical wavelength $\bar{\lambda}_c$. Comparing all the cases in table 1, $\bar{\lambda}_c$ varies within a factor of about 4, i.e. within this factor the critical wavelength is the same for all cases. However, the critical amplification rate, which depends on $\bar{n}_c$, is very sensitive to the value of the surface tension coefficient σ. This sensitivity increases as the fluid is made 'shallower'. Note the change in the exponent of σ in $\bar{n}_c$ when going, in table 1, from cases 1 to 3 and then to 4. The accurate knowledge of the surface tension coefficient σ, and interface viscosity μ_i, is most important in case 4 which is of considerable practical importance for glassy materials which do not have a definite melting point. In this case the importance of having small values of δ, so that the growth rate of the disturbances remains small, cannot be over-emphasized.

6. Effect of variable deceleration during atmospheric entry

In the foregoing analysis it has been assumed that the deceleration g, the characteristic lengths δ or h, and the interface viscosity μ_i, are independent of time. During atmospheric re-entry, however, the deceleration increases with time to a maximum value that occurs after the peak heat transfer rate point along the trajectory has been passed. This variation can be included in the present analysis. The dimensionless equation (23) should be rewritten in dimensional form, so that it is not complicated by the use of reference quantities that are a function of time. If (25) is replaced by

$$\chi = \Phi(\bar{y}) \exp[i\bar{\alpha}\bar{x}] \exp \int_0^{\bar{t}} \bar{n}(\bar{t})\, d\bar{t}, \tag{93}$$

the previous analysis can be retraced in a similar way, yielding an eigenvalue equation for $\bar{n}(\bar{t})$ that can then be made dimensionless, using the time-dependent quantities; $\bar{n}(\bar{t})$ does not depend explicitly on the time, but through $g(\bar{t})$, $\delta(\bar{t})$ or $h(\bar{t})$ and $\mu_i(\bar{t})$, which previously were constants. This extension, therefore, turns out to be very simple.

The amplification ratio will now be given by

$$\eta(\bar{t}, \bar{\alpha})/\eta(0) = \exp \int_0^{\bar{t}} \bar{n}(\tau, \bar{\alpha})\, d\tau, \tag{94}$$

which replaces (1).

At any given time $\bar{t}$, it is of interest to find the value of $\bar{\alpha}$ that maximizes η/η_0 at that instant. That such a maximum exists is obvious; during the re-entry phase when the deceleration increases with time, the maximum amplification will occur at wave-numbers shorter than $\bar{\alpha}_c$, the reason being that shorter wave-numbers are critical at an earlier time and therefore have a longer time to grow. Conversely, during the part of the trajectory where the deceleration decreases with time, longer wave-numbers than $\bar{\alpha}$ will grow to become the largest. However, during this part of the trajectory the heating rates diminish rapidly and the instability problem may become of no practical importance in this flight regime.

The wave-number $\bar{\alpha}$ that will maximize $\eta(\bar{t}, \bar{\alpha})/\eta(\bar{0}, \bar{\alpha})$, at time $\bar{t}$, can be determined from

$$\int_0^{\bar{t}} \frac{\partial \bar{n}(\tau, \bar{\alpha})}{\partial \bar{\alpha}}\, d\tau = 0, \tag{95}$$

where $\bar{\alpha} = 2\pi/\bar{\lambda}$. For any specific problem, (95) will determine the wavelength $\lambda_{\max}(\bar{t})$ that has the largest amplitude $\eta_{\max}(\bar{t})/\eta(0)$ at time $\bar{t}$. Once $\bar{\alpha}_{\max}(\bar{t})$ is known, (94) could be evaluated, probably only by numerical means, to yield $\eta(\bar{t})/\eta(0)$.

7. A numerical example

Before applying the foregoing results to the behaviour of the surface of a body entering the atmosphere, the ablation problem has to be solved. This solution will yield the values of g, δ or h and μ_i needed for the computation of the critical wavelength $\bar{\alpha}_c$ and amplification exponent $\bar{n}_c$, or the maximum quantities $\bar{\alpha}_{\max}(\bar{t})$ and $\bar{\eta}(\bar{t})/\bar{\eta}(0)$. A numerical example follows.

The theory for the ablation of glassy materials has recently been developed by Bethe & Adams (1958). Using their theory, the liquid layer parameters just mentioned were calculated for the stagnation point of a blunt body made of

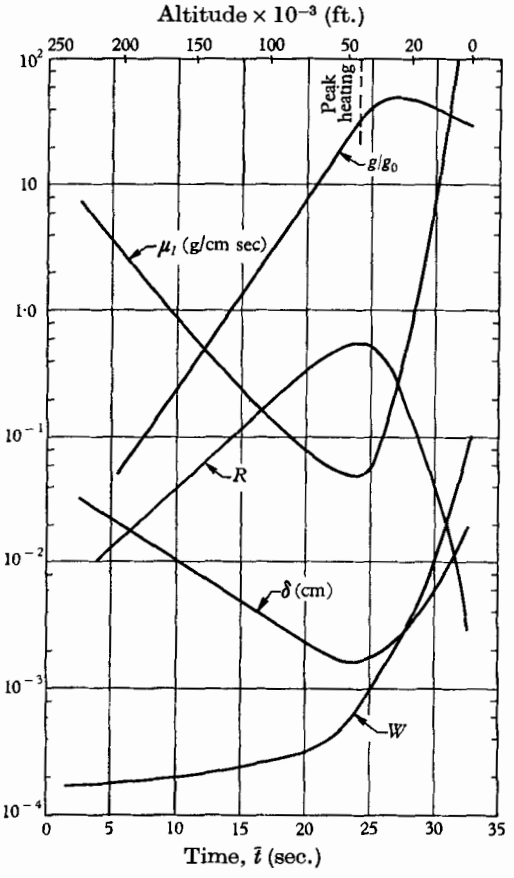

FIGURE 11. Liquid-layer properties at the stagnation point of an ablating Pyrex blunt body entering the atmosphere at ICBM conditions. $g_0 = 980$ cm/sec^2; $R = \sqrt{g}\,\rho_l \delta^{\frac{3}{2}}/\mu_l$; $W = g\rho_l\delta^2/\sigma$. Entry conditions: altitude, 250,000 ft.; velocity, 23,000 ft./sec; angle with horizontal, 21·8°. Ballistic coefficient (mass/$C_D A$): 2,500 lb./ft.^{2}.

pyrex glass entering the atmosphere. The trajectory that we used, calculated by Masson & Gazley (1956), was for an ICBM nose cone entering the atmosphere. The physical properties of Pyrex that we used are:

$$c_{pl} = 0{\cdot}25\,\text{cal/g °K}, \quad k_l = 7 \times 10^{-3}\,\text{cal/cm sec °K}, \quad \rho_l = 2{\cdot}25\,\text{gm/cm}^3,$$

$$\mu_l = \exp\frac{38{,}300}{T(\text{°K})} - 17\,(\text{g/cm sec}),$$

$$p_v = \exp -\frac{46{,}400}{T(\text{°K})} + 14{\cdot}5\,(\text{atm}),$$

$$h_v = 2470\,\text{cal/g}, \quad \sigma = 300\,\text{dynes/cm},$$

where c_{pl}, k_l, p_v and h_v denote, respectively, heat capacity, thermal conductivity, vapour pressure of the liquid and the heat of vaporization of Pyrex. Figure 11

presents the liquid layer properties, g, δ and μ_i as a function of time and flight altitude. W and R were computed from these data. It can be seen from figure 8 that the values of W are sufficiently small so that (65) is valid for the portion of the trajectory considered. Note that n_c/R and R^2 can be obtained from figures 8 and 11, their product satisfying the expression $n_c R \ll 1$ everywhere along the trajectory. This demonstrates that the results of § 2.4 are directly applicable to

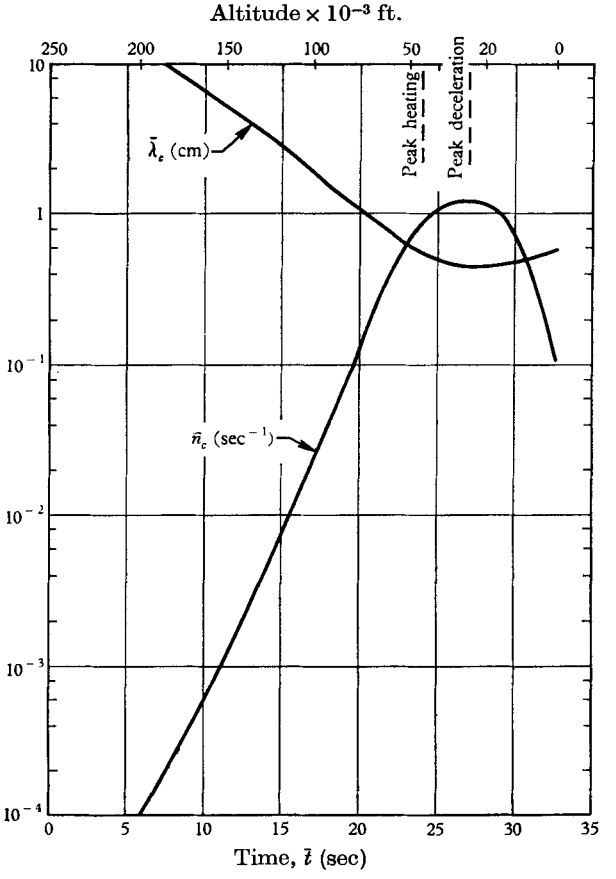

FIGURE 12. Critical amplification factor $\bar{n}_c$ and wavelength $\bar{\lambda}_c$ for the unstable stagnation point liquid layer of an ablating pyrex blunt body entering the atmosphere at ICBM conditions. Entry conditions: altitude, 250,000 ft.; velocity, 23,000 ft./sec; angle with horizontal, 21·8°. Ballistic coefficient (mass/$C_D A$), 2500 lb./ft.^{2}.

our case and that we are justified in using the results of figure 8 and (65). The values of the critical amplification factor $\bar{n}_c$ and wavelength $\bar{\lambda}_c$ are presented in figure 12;† $\bar{n}_c$ increases exponentially with time and then decreases very rapidly when the liquid layer essentially 'freezes' due to the low heat transfer rates encountered after maximum deceleration. Note that the critical wavelength at first decreases, and after peak deceleration starts to increase.

In order to decide whether or not the instability is catastrophic (figure 12), it is necessary to calculate the lifetime of a liquid particle. The life span of a particle

† We have not considered the effects discussed in § 6.

begins when it softens, and ends when the particle either flows away from the blunt portion of the body (where the deceleration is high), or when it becomes vaporized. In the case of Pyrex, only a small amount vaporizes and lifetimes, obtained from the liquid layer calculation, are less than a second for a 1 ft. typical body length. This means that, in the case treated here, the amplification is negligible during most of the trajectory, and that no liquid will be lost due to Lamb–Taylor instability. However, for materials that have a lower viscosity than Pyrex, the situation could be critical. Also, a decrease of the ballistic coefficient (mass/drag coefficient × frontal area) of the entry body increases the instability somewhat.

It should be noted that, although we only calculated the stagnation point conditions, the liquid layer is most unstable in a region away from the stagnation point when the gaseous boundary layer is turbulent. The reason is that although the deceleration normal to the gas-liquid interface diminishes in regions away from the stagnation point, the expression δ^3/μ_i increases sufficiently so that the net effect is to increase the amplification exponent (67) by about 20 %.

8. Concluding remarks

We will next make an attempt to describe the appearance of a blunt axially symmetric body when a thin layer of its surface melts or softens as it enters the atmosphere (figure 2). It is known that in the case of iron or stone meteorites this layer is very thin (Maringer, Simcoe, Manning & Jackson 1958). In the case of stone, the viscosity of the melt will probably be high and the interface velocity will be small. Consider a layer of melted material in the azimuthal $(\bar{x}\bar{y})$-plane (figures 2 and 13*a*). The high enthalpy gas can be imagined to be flowing normal to the page of figure 13*a*. The deceleration provides a mechanism for producing disturbances (figure 1). Liquid from region (*a*) flows to region (*b*). Since the curvature in the azimuthal plane will just perturb the heat transfer from its original value, the heat input stays approximately constant in the azimuthal direction. However, since the protective insulating liquid layer is thinner at (*a*) that at (*b*), the solid will melt more at (*a*) than at (*b*) and therefore develop disturbances of a characteristic wavelength determined by the liquid (figure 13*c*). It should be noted that a liquid layer, however thin, is sufficient for the above described mechanism to produce the azimuthal waves in the solid.

From the discussion in § 6, prior to reaching peak deceleration along the entry trajectory, shorter waves of small amplitude should grow on top of long waves of larger amplitude. The converse statement holds after maximum deceleration.

It should be noted that disturbances in the azimuthal plane will not produce any strong shocks in the supersonic flow around the body, and therefore no localized high heat transfer regions will occur.

In the flow direction, close to the stagnation point, where the liquid velocity vanishes, the instability is of the same wavelength as the azimuthal one. Further away from the stagnation point, the velocities increase and the deceleration normal to the surface decreases. When the product αR^* (where R^* is the liquid Reynolds number based on the interface velocity) is sufficiently large, Feldman (1957) showed that this flow may be stable even under deceleration forces.

One of the problems which we have not treated is the one when the product αR^*, just mentioned, is small. However, it turns out that the flow is stabilized for fairly small liquid velocities.† We should also look into the effect of changing one of the boundary conditions in our problem; we have assumed that the velocity $\bar{v}$, in the $\bar{y}$-direction at $\bar{y} = -\infty$ or $-h$, was zero. In the case of an ablating body this

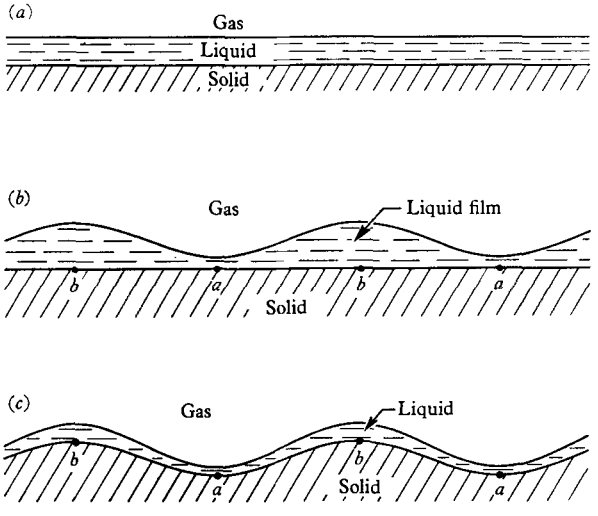

FIGURE 13. Mechanism of production of surface grooves in meteorites due to the liquid film and decelerating forces. *Note*: Flow velocities are normal to the page.

velocity is non-vanishing and corresponds to the ablation velocity. The effect of using a non-vanishing velocity will probably have a small destabilizing effect in the exponential viscosity case. The effect will probably be larger in the case of a liquid layer of finite thickness and constant viscosity.

The physical appearance of the surface of some stone meteorites bears out the qualitative description just made. In the case of iron meteorites, due to the low viscosity of molten iron, the liquid Reynolds numbers may turn out to be much higher than in stony materials, and therefore the liquid layer is hydrodynamically unstable in the flow direction. These disturbances will interact with the gas flow in the subsonic region, and will produce shocks in the supersonic flow which will lead to high local heat transfer rates, and therefore the surface will have, in addition to the azimuthal periodicity, a periodicity in the flow direction $\bar{y}\bar{z}$ (figure 2). This is demonstrated in the photograph of plate 2, figure 14. Of course, stone may possibly, under some conditions, have high liquid Reynolds numbers at extremely high flight velocities, and then it would have also the appearance of an iron meteorite.

In closing, we should emphasize that the analysis presented here is limited to small amplitudes. If for a particular case the amplification η/η_0 turns out to be

† In fact we know that such must be the case because for $R^* = 0$, the flow is unstable due to the Lamb–Taylor mechanism, and for $\alpha R^* > 0$, and sufficiently small, the flow is stable. Therefore, there must be a value of $\alpha R^* > 0$ (i.e. low flow velocities) for which the Lamb–Taylor instability disappears.

large, the problem becomes complicated, since the instability problem is coupled to the heat transfer problem; its solution would lead to the total liquid lost due to instabilities and heat transfer.

This work was sponsored by the Ballistic Missile Division, Air Research and Development Command, U.S. Air Force, under contract AF 04(647)-278. The author wishes to express his appreciation to Professor C. C. Lin, of the Massachusetts Institute of Technology and consultant to the Avco Research Laboratory, for his helpful suggestions and critical discussions. Thanks are also due to Dr Mac C. Adams, Deputy Director of the Avco Research Laboratory, for many helpful discussions that helped to clarify the problem. The author is indebted to Dr John S. Rinehart of the Smithsonian Astrophysical Observatory for pointing out the existence of the meteorites shown in plate 1, figure 1.

REFERENCES

ALLRED, J. C., BLOUNT, G. H. & MILLER, J. H. 1954 *Los Alamos Scientific Lab., Univ. of California Rep.* no. LA-1600.

BELLMAN, R. & PENNINGTON, R. H. 1954 *Quart. Appl. Math.* **12**, 151.

BENJAMIN, T. BROOKE 1957 *J. Fluid Mech.* **2**, 568.

BETHE, H. A. & ADAMS, M. C. 1959 *J. Aero/Space Sci.* **26** (To be published in June issue).

CHANG, C. T. 1956 *Harvard University Division of Engineering and Applied Physics, Combustion Aerodynamics Project interim Tech. Rep.* no. 14.

CHANG, C. T. 1958 Private communication.

FELDMAN, S. 1957 *J. Fluid Mech.* **2**, 343.

LAMB, H. 1932 *Hydrodynamics*, 6th ed. pp. 371, 461. New York: Dover Publications.

LEWIS, D. J. 1950 *Proc. Roy. Soc.* A, **202**, 81.

MARINGER, R. E., SIMCOE, C. R., MANNING, G. K. & JACKSON, L. R. 1958 *Batelle Memorial Institute, Aerodynamic Heating of Iron Meteorites during entry into the Atmosphere.* Contract AF 33(616)-5080.

MASSON, D. J. & GAZLEY, C. 1956 *Aero. Engng Rev.* **15**, no. 11, 45.

SUTTON, G. W. 1958 *J. Aero. Sci.* **25**, 1.

TAYLOR, G. I. 1950 *Proc. Roy. Soc.* A, **201**, 192.

WATSON, B. C. 1957 *Harvard University Division of Engineering and Applied Physics, Combustion Aerodynamics Project interim Tech. Rep.* no. 16.